Histones of Neutrophil Extracellular Traps (NETs) Activate Brain Pericyte via Dectin-1 in Traumatic Brain Injury

Yang-Wuyue Liu
Army Medical University
Jingyu Zhang
Third Military Medical University Daping Hospital and Research Institute of Surgery
Wanda Bi
Army Medical University
Mi Zhou
Army Medical University
Jiabo Li
Chongqing University
Tiantian Xiong
Army Medical University
Nan Yang
Third Military Medical University Daping Hospital and Research Institute of Surgery
Li Zhao
Army Medical University
Xing Chen
Third Military Medical University Daping Hospital and Research Institute of Surgery
Yuanguo Zhou
Third Military Medical University Daping Hospital and Research Institute of Surgery
Wenhui He
Army Medical University
Teng Yang
Army Medical University
Hao Wang
Third Military Medical University Daping Hospital and Research Institute of Surgery
Lunshan Xu
Third Military Medical University Daping Hospital and Research Institute of Surgery
Shuang-Shuang Dai (tmmubiodss66@aliyun.com)
Third Military Medical University https://orcid.org/0000-0002-1394-5471

Research

Keywords: Pericyte, Neutrophil, TBI, NETs, Dectin-1

Posted Date: May 12th, 2022

DOI: https://doi.org/10.21203/rs.3.rs-827730/v2

Abstract

Brain pericyte is unique and indispensable part of blood-brain barrier (BBB), and contributes to several pathological processes in traumatic brain injury (TBI). However, the cellular and molecular mechanisms about how pericyte is regulated in damaged brain are largely unknown. Here, we show that neutrophil extracellular traps (NETs) formation induces the appearance of $CD11b^+$ pericytes post TBI. These $CD11b^+$ pericytes subsets are characterized with increased permeability and pro-inflammatory profiles compared to $CD11b^-$ pericytes. Moreover, histones from NETs by Dectin-1 facilitate CD11b induction on brain pericytes in PKC-c-Jun dependent manner, conferring neuroinflammation and BBB dysfunction post TBI. These data indicate that "neutrophil-NETs-pericyte" and "histones-Dectin-1-CD11b" are possible mechanisms for pericyte's activation and dysfunction. Targeting at NETs formation and Dectin-1 are promising ways for TBI treatments.

Introduction

The overwhelming lymphocyte infiltration and dysfunction of blood-brain barrier (BBB) are two important pathophysiologic mechanisms of traumatic brain injury (TBI) [1]. Neutrophils are the most abundant circulating leukocytes that migrate at the injury sites, and involved in the initiation and development of immunological response [2-4]. It was previously shown that BBB disruption facilitated neutrophils infiltrating into brain tissue [5]. However, the cellular and molecular mechanisms about how BBB lost its “brain guard” functions and interacted with neutrophils post TBI are still less-explored.

BBB is compact and dense capillary wall that allows few substances going through to the brain, which is made up by endothelial cells, pericytes and astrocytes [6]. Pericytes are surrounded by endothelial basement membrane and astrocytic pseudopodia [7]. Of note, pericytes are sensitive and versatile toward inflammatory stimulus, regulating cerebral blood flow dynamics and leukocyte recruitment under pathological conditions [8, 9]. Proebstl D *et al* found that pericytes were the accomplice toward neutrophils under inflammatory conditions, losing its guard function and supporting neutrophil subendothelial crawling [10]. Brain pericytes were also possibly induced to express CD11b, a transmembrane protein found on macrophage and microglia, to form microglia-like phenotype in stroke and AD model [11, 12]. However, if CD11b-expressing ($CD11b^+$) pericytes were formed and functioned in BBB disruption during TBI is undetermined.

Neutrophil extracellular traps (NETs) are characterized as decondensed chromatin, perforated membrane and spilled nucleoplasm in activated neutrophils. NETs are fundamental weapons for neutrophils catching and killing pathogens, as well as contributors to unintended damages [13, 14]. It is recently reported that NETs contribute to the initiation and development of several diseases in central nervous system (CNS) [15-17]. NETs formation markers, including citrullinated histone H3 (CitH3), neutrophil-derived DNA segments and peptidylarginine deiminase 4 (PAD4) are significantly increased after TBI or stroke [17, 18]. Vaibhav K *et al* presented that NETs were key factors to exacerbate TBI severity through aggravating neurovascular injury [18]; Yipp BG *et al* proved that NETs generally formed during crawling

and transmigrating, casted large interacted areas with vascular units/BBB [19]. Therefore, NETs are highly involved in BBB disruption and possibly facilitate neutrophil-pericyte interaction.

In this study, we explored the possible relationships between that NETs formation and appearance of $CD11b^+$ pericytes in TBI model. The molecular mechanisms of $CD11b^+$ pericytes formation in damaged brain tissues were further investigated, which might provide better understanding of pericyte-neutrophil interactions and BBB dysfunctions in TBI pathogenesis.

Materials And Methods

TBI patients: All studies were approved by the Institutional Research Ethics Committee of Army Medical University, and written informed consent was obtained from each patient's relatives in Department of Neurosurgery, Daping Hospital (Army Special Medical Center). Brain specimens were collected from acute middle/severe TBI patients (GCS of 3-9, within 24 hours) while decompressive craniectomy and damaged brain tissue resection were necessary for patients to survive (Table S1). All samples were de-identified and coded by the attending surgeon before transport to the laboratory. The specimens were acquired and processed based on Clinical Investigation Ethical Approval from Army Medical Center (2021004, person in charge: Zhang Jingyu), and stored according to the Principles of Human Samples Preservations from PRC.

TBI mice model: All animal procedures were approved by The Institutional Animal Care and Use Committee at Army Medical University. Adult mixed-sex C57/BL6 mice (age from 6-8 weeks) were provided by Animal Center of Army Medical University and subjected to sham or controlled cortical impact as we did previously [20]. Briefly, mice were anesthetized using pentobarbital sodium (30mg/kg) and craniotomy was made in the left parietal bone midway (anterior-posterior 2 mm, medial-lateral 2 mm from bregma). The exposed cortex was impacted by automatic BSI impact machine (LinTech, Monrovia, CA, USA) with down stroke (velocity: 2.5 m/s, deformation depth: 3 mm, duration: 150 ms) to construct moderate TBI mice model. Sham-operated mice underwent the same anesthetic and surgical procedures without impact. The skin incision was closed by sterile sutures and mice were put back to clean, warm cage to recover. For drug treatment studies, Laminarin (TLRL-LAM, InvivoGen) and Cl-amidine (S8141, Selleck Chem) dissolved by saline was administered every three days via intraperitoneal injection.

Neutrophil isolation and treatment: Murine neutrophils were isolated from bone marrow as we did before [21]. The purity of harvested cells was more than 98% which was confirmed by FACS with specific markers ($CD11b^+LY6G^+$). Isolated neutrophils were washed with cold PBS for three times and resuspended in Dulbecco's modified Eagle medium (DMEM), containing high glucose and antibiotics without FBS. Neutrophils were treated with/without PMA (100ng/ml, P1585, Sigma-Aldrich) for 30 min. Then, stimulated neutrophils were washed with DMEM for 3 times and cultured with new DMEM medium (antibiotic and FBS free) for another 6 hours. The supernatant was harvested by low speed centrifuge

(1500rpm, 5min, 4°C) and purified with high speed centrifuge (14000rpm, 20min, 4°C) to remove cell debris. The medium ratio of NETs-formed medium/ new DMEM was 1:3 according to preliminary test (Figure S1a, S1b). Under this condition, the medium could induce obvious CD11b expression without obvious cytotoxicity.

Culture of murine brain pericyte cell line: The cell line of mouse brain vascular pericytes (MBVP) was purchased from ScienCell Research Laboratories (M1200, San Diego). MBVP cells were cultured with DMEM at subconfluent density according to the supplier's protocol. Histone peptides of Histone 1 (H1917), Histone 3 (12-357) and Histone 4 (12-347) were all purchased from Sigma-Aldrich and dissolved in ddH_2O for the following treatments.

Brain tissue preparation and analytic fluorescence activated cell sorting (FACS): Mice were sacrificed with CO_2 prior to brain dissection. FACS sorting of brain pericytes was performed according to previous study [22]. In Brief, brain tissue was dissected from mice perfused with saline transcardially and digested with Liberase™ TL Research Grade (05401020001, Sigma Aldrich) and 2 μg/ ml DNase I (104159, Roche) for 30 min at 37 °C. Cell suspensions subsequently were homogenized with grinder and filtered with sieve (200 mesh) to remove undigested tissue blocks. Myelin and debris were removed by 22% Percoll (P4937, Sigma-Aldrich) centrifugation for 10 min, 560×g at 4 °C. Pellets with single vascular cells were carefully collected and resuspended with PBS containing 2% FBS. Single cell suspensions from brain tissues and cell lines were stained for 30 min at 4 °C with specific antibodies (Table S2). Flow cytometry data were analyzed with FlowJo software version 11.

Pericyte sorting from brain: After constructing TBI model, single cell suspension and antibody incubation from brain tissues were achieved as FACS. Infiltrated immune cells ($CD45^+$) were excluded before pericytes sorting. $CD11b^+$ and $CD11b^-$ pericyte populations were further collected respectively. These sorted cells were washed with PBS (antibiotic contained) for three times and cultured with complete DMEM medium in 24-well plate.

Transwell experiment: Sorted pericytes were seeded in 24-well plate and cultured for 24 hours. Transwell inserts (polyester membranes, 8μm pore size, ø=6.5mm; Corning, NY, USA) were put into plate with freshly isolated neutrophils (10^6) added into upper side. After coculturing for 12 hours, migrated neutrophils on lower side of Transwell insert were harvested and visualized by Giemsa staining (48900, Sigma-Aldrich). The stained cells were counted by Image J.

Western blotting: Whole-cell lysates were collected and prepared as we did before [21], and western blot procedure was carried out by standard methods. The information of antibodies for specific proteins were listed in Table S2. The quantification of target bands was achieved by Image J.

LC-MS analysis of cell metabolites: A liquid-liquid extraction and liquid chromatography-electrospray ionization tandem mass spectrometry (LC-MS) method was utilized to determining metabolites from cell culture media. Primary isolated murine neutrophils were treated with or without PMA (100ng/ml) for 30

min, then incubated with DMEM (antibiotic and FBS free) for 6 hours. Subsequently, cultured medium was collected by high speed centrifuge and lyophilized for following steps [23]. Each group contains 7 individual samples and differential molecules with p value<0.05 were screened out.

TMT proteomics analysis of cell cultured medium: Tandem Mass Tags (TMT) labeled quantitative proteomics method was performed to analyze total protein in neutrophil-cultured medium. Proteins with changes greater than 1.5-fold and $p < 0.05$ were considered differentially expressed, and bioinformatics analysis was performed subsequently as previously [24].

Immunohistochemitry: For tissue sections, mice were perfused with 0.9% NaCl transcardially after anesthetization. Then the brain tissues were immediately frozen and embedded with OCT (4583, Tissue-Tek). Brain sections (10μm) were incubated with primary antibodies (Table S2) diluted by 5% BSA (V900933, Sigma-Aldrich) containing 0.1% Triton X-100 (T8787, Sigma-Aldrich). Finally, samples were stained with DAPI and intended secondary antibodies and photographed by fluorescence microscope (Olympus IX-81).

Quantitative Realtime-PCR: Total RNA extraction of intended cells was achieved by TRIzol Reagent protocol (15596018, Thermo Fisher). RNA samples were reverse transcribed to cDNA using a Reverse Kit (DRR047S, Takara). Quantitative reverse transcription polymerase chain reaction (qRT-PCR) was performed on a Bio-Rad iCycler (Version 3.0A). The ΔΔCt method was used to calculate relative mRNA levels in treatment groups compared to control group. Primer sequences were listed in Table S3.

TEER measurement: Transwell inserts (polyester membranes, 3μm pore size, ø=6.5mm; Corning, NY, USA) were coated with pericyte cell line MBVP in 24-well plate ($10^5/cm^2$). The Millicell-ERS (Electrical Resistance System, MERS00002, Millipore) was inserted between upper chamber and lower well while measurement took place. TEER values were obtained from continuous impedance measurements as described previously [25]. Once the TEER value of each insert reached above $200Ω/cm^2$ (typically after 2-3 days), cells were treated with NETs-induced medium as described above or combined with other treatments (as shown in figures), and TEER measurements were obtained every two hours. TEER data were recorded as $Ω/cm^2$ and presented as percentage (%) by comparing to the value of control group at the beginning.

Evans Blue assay: 2% Evans Blue solution (4 mL/kg, E8010, Solarbio) was IV injected after TBI. The stain was allowed to circulate for 30 minutes, 6 or 24 hours. Afterwards, the mice were sacrificed and transcardially perfused with 50ml of ice-cold PBS. The left injured brain hemisphere was removed and weighed. Then brain tissues were homogenized in 1ml PBS, centrifuged for 30 min (14000 rpm at 4°C). Equal amount of 50% trichloroacetic acid was added to each 500μl supernatant and incubated over night at 4° C. Supernatant was subsequently centrifuged (30 min, 14000rpm at 4°C) and measured by Infinite

M200 plate reader (excitation at 620; emission at 680). Free PBS combined with 50% trichloroacetic acid was regarded as blank, and gradient doses of Evans Blue were measured to draw the standard curve. The results were quantified according to standard curve and presented as (μg of Evans Blue stain)/(g of brain tissue).

Plasmids construction: The 5'-UTR sequence of mouse *CD11b* gene was achieved using Pubmed (http://www.ncbi.nlm.nih.gov/entrez/). The 5'-UTR sequence of mouse *CD11b* gene was further analyzed for potential c-Jun (AP-1) binding sides by using web-based algorithm (NUBIScan and hTFtarget) as we did before [26]. Mouse *CD11b* gene promoter region containing fragment (−2900 to +190) was chemically synthesized by Sangon (Shanghai, China) cloned into pGL3-basic vector. All the resulting plasmids were named as pGFs as Figure 8A shows.

Dual-luciferase reporter assay: Murine brain pericyte cell line MBVP was transiently transfected with reporter plasmids (pGFs) by Lipofectamine 3000 (L3000008, Thermo Fisher). Two hours later the cultured medium was replaced with fresh complete DMEM medium. After 24 hours incubation, NETs-formed or normal medium was added with specific drugs for another 24 hours. Then the cell lysates were collected and luciferase activities were measured by Dual-Luciferase Reporter System according to the instruction (E1910, Promega). The transfection experiments were repeated three times in triplicate, and the transfection efficiency was normalized by dividing firefly luciferase activity to renilla luciferase activity.

Chromatin immunoprecipitation assays: Chromatin immunoprecipitation (ChIP) assays were performed with Pierce™ ChIP assay kit (26157, Thermo Fisher) according to the manufacturer's instructions. The targeted protein-DNA mixture was gathered by PureProteome Magnet (LSKMAGS08, Millipore). Then the final DNA extracts were analyzed by Realtime-PCR with specific primers (Table S4). The antibodies against c-Jun and the control IgG were obtained from CST and Beyotime respectively (listed in Table S2).

Neurobehavioral evaluations: *Open-field test:* Mice were tested in a square box (40cm × 40cm × 40cm) for 10 min, and activity was digitally recorded as we did before [27]. Travel distance, mean velocity, and time spent in the center zone were analyzed with Ethovision XT video-tracking software (Noldus Information Technology, Asheville, NC). *Foot-fault test*: The experiments were carried out on an elevated beam (2.5 × 75 cm) raised 76 cm above the floor as previously described [28]. Mice were placed at the beginning of the beam and their movements were manual from the beginning to the end. It was considered an individual foot fault when a mouse paw slipped completely through the beam during its walking. The average foot fault score was calculated from the total steps within 75cm in three separate trials.

Statistical analysis: All data were analyzed and presented by using GraphPad Prism version 5.01 (GraphPad Software). Unpaired two-tailed Student *t* test were evaluated for comparison of treated groups with vehicle controls. For analyzing parameters depending on two factors or more, two-way ANOVA/multivariate analysis of variance (MANOVA) was used with Bonferroni correction. A p value < 0.05 was considered statistically significant. Data in figures were all represented as mean ± SEM with *p < 0.05; **p < 0.01; ***p < 0.001. The number of animals and experimental repeats were marked in the corresponding figure legends.

Results

CD11b$^+$ pericytes are detected in brain from TBI patients and mice, which are characterized with pro-inflammatory profiles.

Previous studies have shown that CD11b$^+$ pericyte is associated with enhanced phagocytosis capacity and BBB disruption in AD model or stroke model [11, 12]. However, the presence of CD11b$^+$ pericyte in TBI model is still undetermined. Using triple-labeling immunofluorescence, we confirmed the existence of CD11b$^+$ pericyte (marked with PDGFRβ or α-SMA, white arrows) in brain from TBI patient (Figure 1a&1b) and mice (Figure 1c&1d, injured sites were highlighted with dotted lines). Next, we used FACS to specifically distinguish brain pericytes (CD45$^-$CD31$^-$CD13$^+$) from brain tissue according to previous study [22] (Figure 2a) and results showed that CD11b$^+$ pericytes was significantly increased in damaged brain 24 hours post TBI compared to Sham (Figure 2b, 2c, S1c). In order to explore the differences between CD11b$^+$ and CD11b$^-$ pericytes, we sorted these two pericyte subpopulations from damaged brains of TBI mice and prepared for RNA-sequence and Transwell experiment. As shown in Figure 2d, CD11b$^+$ pericytes were more robust to attract neutrophils to migrate across the membrane compared to CD11b$^-$ pericytes. RNA-sequencing further presented that mRNA levels of pro-inflammatory genes (*TNF-α, IL-1β, CCL2/5, CXCL8/10*) and BBB disruption-related molecules (*MMP2 and MMP9*) in CD11b$^+$ pericytes were significantly higher than that in CD11b$^-$ pericytes (Figure 2e, 2f&S2). Meanwhile, we rechecked the RNA-seq data and found that these sorted pericyte expressed relatively low mRNA levels of CD163 (macrophage marker gene) and TMEM119(microglia marker gene), indicating these cells were neither BBB-associated macrophage nor microglia (Figure 2f). The increased mRNA levels of pro-inflammatory molecules (*TNF-α, IL-1β, CCL5 and MMP9*) in CD11b$^+$ pericytes were also verified by Realtime-PCR (Figure 2g). These data provided the evidences that percentage of CD11b$^+$ pericytes in brain after TBI was obviously increased and characterized with pro-inflammatory profiles. These CD11b$^+$ pericytes are possibly important contributors for neuroinflammation and BBB disruption in TBI pathogenesis.

NETs formation is enhanced in TBI and NETs-formed medium significantly induces CD11b expression in pericytes.

It has been proven that NETs formation is highly increased under inflammatory conditions [17, 18]. Our data reiterated the conclusion that neutrophils in blood from TBI mice were more easily to form NETs structure toward PMA stimulation (Figure 3a). FACS experiment further showed that NETs formation percentage ($CD11b^+LY6G^+MPO^+$ $CitH3^+$) from brain parenchyma of TBI mice was relatively high (Figure 3b-3d), which was in consistency with Vaibhav K's work [18]. Meanwhile, the neutrophil infiltration rate was positively related with the frequency of $CD11b^+$ pericyte in damaged brain tissue (Figure 3e). Thus, we speculated if NETs formation was related to CD11b induction on pericytes. To confirm this hypothesis, we treated pericyte cell line (MVBP) with NETs-formed medium at established conditions (obvious effects without strong cytotoxicity according to Figure S1). After culturing with NETs-induced medium (PMA) for 48 hours, FACS analysis showed that CD11b expression was strongly induced in MVBP (Figure 4a&4b). Immunofluorescence, WB, and Realtime-PCR experiments also supported that NETs-formed medium increased CD11b expression and decreased tight-junction protein ZO-1 levels *in vitro* (Figure 4c-4e). TEER experiment further showed that NETs-formed medium dramatically jeopardized pericyte integrity (Figure 4f). All the effects mediated by NETs-induced medium could be inhibited by Cl-Amidine (NETs formation inhibitor by decreasing PAD activity), suggesting that NETs formation was associated with CD11b induction in pericytes.

Histones are the main components of NETs to drive CD11b induction in pericytes.

We next aimed to investigate what components of NETs-formed medium drove CD11b induction in pericytes. In Figure 5a, we collected the cultured medium after removing neutrophils with or without PMA stimulation for proteomics and metabolomics analysis. In proteomic analysis, overall 4098 proteins were identified in these two groups. Proteins with repeatable fold changes >1.2 or <0.8 were screened out as differentially expressed molecules (Figure 5b, S2). In PMA-stimulated groups, there were 101 up-regulated and 3 down-regulated proteins identified. Of note, histones accounted for 30% of the top up-regulated proteins and other neutrophil intracellular molecules (lactoferrin, complement 3, and metalloproteinase *et al*) were also detectable, which was consistent with reported NETs characters [14]. NETs formation induced by PMA caused dramatic alterations in amino acids too, such as N-acetyl-L-cycteine, L-isoleucine, L-glutamate (Figure 5c&S3). In order to testify their effects on pericytes, we selected some of these proteins (histones and lactoferrin) or metabolites (N-acetyl-L-cycteine and L-isoleucine) to confirm if they could change CD11b expression *in vitro*. As shown in Figure 5d, histones could increase CD11b mRNA levels after 24 hours treatment. WB and FACS analysis also proved that histone treatment mediated CD11b induction and ZO-1 downregulation on pericytes in dose dependent manner (Figure 5e&5f). We did not see obvious alterations in CD11b mRNA levels (Figure S4) under specific concentrations of lactoferrin, N-acetyl-L-cycteine and L-isoleucine according to previous studies [29, 30], indicating that these metabolites/amino acids were not possible factors to drive CD11b induction in pericytes.

Dectin-1 is fundamental for pericyte to respond toward histones of NETs *in vitro*.

After defining histones as the main components of NETs to affect pericytes, we aimed to decipher the possible ways that pericytes might respond to. According to previous study, we converted our attention to C-type lectin receptors (CLRs), a large family of transmembrane receptors that recognized not only fungal moieties, but also histone-related molecules from dead cells [31, 32]. Three types of CLRs are classified based on their molecular structures: type I, type II and soluble type. Of which, Type II CLRs are the main receptors for recognition of histone sequences or histone deacetylase complexes released from disintegrated DNA [31, 33]. Type II CLRs carry a conserved carbohydrate-recognition domain and contain five receptors: Dectin-1, Dectin-2, macrophage-inducible CLR (Mincle), dendritic cell-specific ICAM3-grabbing nonintegrin (DC-SIGN), as well as DC-NK lectin group receptor-1 (DNGR-1) [34]. Based on human protein atlas database (https://www.proteinatlas.org/), the expressions of type II CLRs in CNS (yellow bars) were relatively low except Dectin-1 and DNGR-1 (Figure S5a). The protein expression and glycosylation level of Dectin-1 was obviously upregulated in MVBP with PMA-induced medium or histones (Figure 6a). This proved that Dectin-1 expression was positively related to CD11b upregulation in brain pericytes. In order to confirm if Dectin-1 was responsible for CD11b upregulation, the Dectin-1 siRNAs and specific antagonist Laminarin (LAM) were introduced in the following experiments. WB showed that synthetic siRNAs was capable to interfere Dectin-1 protein expression in the presence of NETs-medium and histones (Figure 6b). Antagonizing Dectin-1 by LAM as well as blocking Dectin-1 expression by siRNAs decreased CD11b mRNA levels compared to PMA-medium alone (Figure 6c&6d). This phenomenon was consistent with histones-treated groups (Figure 6e&6f). TEER experiments also confirmed that blocking Dectin-1 (LAM or siRNAs) was beneficial for restoring pericyte integrity *in vitro* (Figure 6g&6h). These results showed that Dectin-1 antagonist LAM and siRNAs were competent to blunt CD11b expression mediated by NETs medium or histones stimulation, confirming that Dectin-1 was indispensable for pericytes to react toward histones of NETs.

PKCζ/λ and c-Jun activation mediated by Dectin-1 are responsible for CD11b induction of pericytes during NETs and histones treatments.

Next, we explored the possible signaling pathways mediated by Dectin-1 that were involved in CD11b induction. After reading previous literature, we sorted out that protein kinase Cζ/λ (PKCζ/λ) and transcriptional factor c-Jun were possible molecules post Dectin-1 activation [34]. The levels of phosphorylated PKC (p-PKCζ/λ) and phosphorylated c-Jun (p-c-Jun), activation status of these two molecules, were significantly increased following NETs-formed medium or histones treatment (Figure 7a&7b). In the presence of Dectin-1 inhibitor LAM, Dectin-1 siRNAs and PKC inhibitor GFX, the phosphorylation levels of PKCζ/λ and c-Jun dropped dramatically (Figure 7a&7b), showing that Dectin-1 was essential for PKCζ/λ and c-Jun activation toward NETs-medium or histones stimulation. Realtime-PCR demonstrated that both PKC inhibitor and c-Jun inhibitor blunted CD11b induction mediated by NETs medium or histones (Figure 7c). These data proved that Dectin-1 contributed to CD11b upregulation

expression in pericytes toward NETs-formed medium/ histones through mediating PKCζ/λ-c-Jun signaling pathway.

c-Jun directly binds to the promoter sequence of *CD11b* to enhance its expression in pericytes.

c-Jun is an important transcription factors that modulating gene expression through binding to promoter region. We next tested if c-Jun could activate *CD11b* transcription by binding to its promoter gene. After searching the possible c-Jun binding sites in *CD11b* promoter gene region by NUBIScan, we screened out two possible sites with the “TGACTCA” motif (Figure 7d&S6). Subsequently, three luciferase reporters containing different promoter regions of *CD11b* gene were constructed, as well as two mutation luciferase reporters that disrupted binding motif. They were named as pGF1 (-2900 to +190), pGF2 (-1000 to +190), pGF3 (-200 to +190), pGFmut1(-1250 to -1244) and pGFmut2 (-410 to -403) respectively (Figure 7d). Then luciferase reporter assays showed that the activity of pGF1 and pGF2 was significantly increased in the presence of NETs-formed medium or histones (Figure 7e), revealing that these two potential binding sites of *CD11b* promoter region were capable to promote *CD11b* gene expression. Of note, the ability of histones to raise *CD11b* promoter activity was relatively low compared to NETs-formed medium (Figure 7e), indicating that there were other potential components in NETs that induced CD11b expression apart from histones. Moreover, mutating these two sides separately both decreased the promoter activity (Figure 7f), verifying that these two binding sites were required for CD11b induction. ChIP assays further confirmed that c-Jun could bind to these two *CD11b* promoter regions (SF1:-1250 to -1244, SF2:-410 to -403, primers were shown in Table S4) after stimulation of NETs-formed medium or histones (Figure 7g-7i). Taken together, these results indicated that c-Jun activated CD11b expression by binding to two sites (-1250 to -1244, -410 to -403) in *CD11b* gene promoter region.

Inhibiting NETs formation and blocking Dectin-1 both improve brain function recovery after TBI.

Previous study and our results above confirmed that NETs formation and brain pericyte dysfunction contributed to acute TBI pathogenesis [18]. We further proved that histones of NETs facilitated CD11b induction on pericytes in Dectin-1/PKC/c-Jun pathways. It had been shown that blocking Dectin-1 was beneficial for ischemia injury in heart and brain [35, 36]. However, if blocking NETs formation and inhibiting Dectin-1 could decrease pericyte activation, restore BBB integrity and improve TBI long-term outcomes were undetermined. Thus, we explored the effects of Cl-Amidine (NETs inhibitor) and LAM (Dectin-1 antagonist) at different time points after TBI (Figure 8a). The mice were treated with or without Cl-Amidine (50mg/kg) and LAM (25 mg/kg and 50mg/kg) intraperitoneally every three days post TBI according to previous study [18, 35]. Administration of Cl-Amidine and LAM significantly reduced BBB permeability and death rate compared with saline group in acute phase (Figure 8b&8c). These two drugs also improved motor and psychiatric functions in TBI mice after two/four weeks (Figure 8d-8f). FACS results also showed that Cl-Amidine and LAM dramatically decreased the amounts of infiltrated

neutrophils (Figure 8g&8h) and $CD11b^+$ brain pericytes from injured brains within 24h post TBI (Figure 8i&8j), result of neurobehavioral improvement. These data provided the evidences that targeting at NETs formation and Dectin-1 were effective to ameliorate BBB disruption and neutrophil infiltration, facilitating neurological recovery after TBI.

Discussion

In this study, we for the first time report that histones of NETs induce CD11b expression in brain pericytes. The $CD11b^+$ pericytes express higher pro-inflammatory molecules and decreased integrity compared to $CD11b^-$ pericytes, leading to BBB disruption and increased leukocyte infiltration. Mechanistically, Dectin-1 in pericytes is responsible for recognizing histones to induce CD11b expression in PKC-c-Jun dependent manner. These data indicate that NETs formation is associated with BBB disruption by inducing CD11b expression in brain pericytes. “Neutrophils-NETs-pericytes” and “histones-Dectin-1-CD11b” are possible cellular and molecular mechanisms for building connection between BBB disruption and neutrophil infiltration.

Pericytes are generally treated as indispensable participants during angiogenesis and microcirculation regulation [7, 37]. Under pathological conditions, activated pericytes could mediate neuroinflammation through diverse ways, including leukocyte recruitment and BBB disruption [9], pericyte-endothelium communications [38], fibrotic scarring formation [39], as well as endocytosis [40]. Hence, more functions and phenotypes that $CD11b^+$ brain pericyte might exhibit within TBI pathogenesis are desperately needed in the future study.

In brain diseases, it has been shown that NETs are associated with cerebral edema, hypoperfusion, BBB damage, neurotoxicity, amyloid β plaque deposition and so forth [15, 18]. Previous studies have shown that circulating histones from necrotic or dead cells are highly associated with several brain diseases [41, 42]. Our study builds the connections between NETs histones and CD11b induction in brain pericytes, providing possible histone-related molecular mechanism in neuroinflammation. Of note, there are two forms of NETs structure, including suicidal NETosis and vital NETosis [43]. For suicidal NETosis, dead neutrophils spill out the segmented chromatins and intacellular granules. While vital NETosis generally forms when neutrophils remain live and release only parts of their nuclear or mitochondrial DNA and does not contain antibacterial proteins and granules [44]. In present study, we mainly focused on the on the effects mediated by extracellular spills when soluble NETs (suicidal NETosis) were formed. The differences of extracellular components and effects between vital NETosis and suicidal NETosis would be interesting to explore.

Previous study and our data (Figure S5b& S5c) showed that histones contained some amino acid residues such as lysine, arginine, and histidine were critical for being recognized by Clec2d [31]. We speculate Dectin-1 might bind to histones dependent on these residues since Dectin-1 and Clec2d share similar binding domain (Figure S5b), which needs to be verified in the future. Based on the latest study, Dectin-1 was highly enhanced in brain tissue following ischemic injury or TBI, causing overwhelming

activation of microglia [35, 45]. This provides the hint that Dectin-1 might affect neuroinflammation in multiple ways. Li X *et al* also found that Dectin-1 facilitated CD11b activation by forming Vav-PLCγ complex during fungal clearance [46], provides the possibility that Dectin-1 modulated CD11b functions though changing either expression level or activation status.

In conclusion, our data support that NETs-associated histones promote $CD11b^{+}$ brain pericytes formation in TBI. Recognition of histones by Dectin-1 on pericytes contributes to CD11b induction in PKC-c-Jun dependent manner. Targeting at NETs formation and Dectin-1 are efficient ways for restoring BBB integrity and decreasing neutrophil infiltration to improve neurological outcomes of TBI.

Declarations

Acknowledgement: This work was supported by National Natural Science Foundation of China (32000670, 82071779) and Chongqing Research Program of Basic Research and Frontier Technology (cstc2017jcyjAX0338).

Conflict of interest: The authors all declare that they have no competing interest.

References

1. Luo J, Wu X, Liu H, Cui W, Guo W, Guo K, *et al*. Antagonism of Protease-Activated Receptor 4 Protects Against Traumatic Brain Injury by Suppressing Neuroinflammation via Inhibition of Tab2/NF-κB Signaling. Neurosci Bull 2021, 37: 242-254.

2. Jing Y, Yang DX, Wang W, Yuan F, Chen H, Ding J, *et al*. Aloin Protects Against Blood-Brain Barrier Damage After Traumatic Brain Injury in Mice. Neurosci Bull 2020, 36: 625-638.

3. Williams OH, Tallantyre EC, Robertson NP. Traumatic brain injury: pathophysiology, clinical outcome and treatment. J Neurol 2015, 262: 1394-1396.

4. Kolaczkowska E, Kubes P. Neutrophil recruitment and function in health and inflammation. Nat Rev Immunol 2013, 13: 159-175.

5. Shi Y, Zhang L, Pu H, Mao L, Hu X, Jiang X, *et al*. Rapid endothelial cytoskeletal reorganization enables early blood-brain barrier disruption and long-term ischaemic reperfusion brain injury. Nat Commun 2016, 7: 10523.

6. Liebner S, Dijkhuizen RM, Reiss Y, Plate KH, Agalliu D, Constantin G. Functional morphology of the blood-brain barrier in health and disease. Acta Neuropathol 2018, 135: 311-336.

7. Sweeney MD, Ayyadurai S, Zlokovic BV. Pericytes of the neurovascular unit: key functions and signaling pathways. Nat Neurosci 2016, 19: 771-783.

8. Smyth L, Rustenhoven J, Park TI, Schweder P, Jansson D, Heppner PA, *et al*. Unique and shared inflammatory profiles of human brain endothelia and pericytes. J Neuroinflammation 2018, 15: 138.

9. Rustenhoven J, Jansson D, Smyth LC, Dragunow M. Brain Pericytes As Mediators of Neuroinflammation. Trends Pharmacol Sci 2017, 38: 291-304.

10. Proebstl D, Voisin MB, Woodfin A, Whiteford J, D'Acquisto F, Jones GE, *et al*. Pericytes support neutrophil subendothelial cell crawling and breaching of venular walls in vivo. J Exp Med 2012, 209: 1219-1234.

11. Hutter-Schmid B, Humpel C. Primary mouse brain pericytes isolated from transgenic Alzheimer mice spontaneously differentiate into a CD11b(+) microglial-like cell type in vitro. Exp Gerontol 2018, 112: 30-37.

12. Özen I, Deierborg T, Miharada K, Padel T, Englund E, Genové G, *et al*. Brain pericytes acquire a microglial phenotype after stroke. Acta Neuropathol 2014, 128: 381-396.

13. Yipp BG, Kubes P. NETosis: how vital is it? Blood 2013, 122: 2784-2794.

14. Tan C, Aziz M, Wang P. The vitals of NETs. J Leukoc Biol 2021, 110: 797-808.

15. Manda-Handzlik A, Demkow U. The Brain Entangled: The Contribution of Neutrophil Extracellular Traps to the Diseases of the Central Nervous System. Cells 2019, 8.

16. Kang L, Yu H, Yang X, Zhu Y, Bai X, Wang R, *et al*. Neutrophil extracellular traps released by neutrophils impair revascularization and vascular remodeling after stroke. Nat Commun 2020, 11: 2488.

17. Zeng H, Fu X, Cai J, Sun C, Yu M, Peng Y, *et al*. Neutrophil Extracellular Traps may be a Potential Target for Treating Early Brain Injury in Subarachnoid Hemorrhage. Transl Stroke Res 2021.

18. Vaibhav K, Braun M, Alverson K, Khodadadi H, Kutiyanawalla A, Ward A, *et al*. Neutrophil extracellular traps exacerbate neurological deficits after traumatic brain injury. Sci Adv 2020, 6: x8847.

19. Yipp BG, Petri B, Salina D, Jenne CN, Scott BN, Zbytnuik LD, *et al*. Infection-induced NETosis is a dynamic process involving neutrophil multitasking in vivo. Nat Med 2012, 18: 1386-1393.

20. Yang T, Liu YW, Zhao L, Wang H, Yang N, Dai SS, *et al*. Metabotropic glutamate receptor 5 deficiency inhibits neutrophil infiltration after traumatic brain injury in mice. Sci Rep 2017, 7: 9998.

21. Liu YW, Yang T, Zhao L, Ni Z, Yang N, He F, *et al*. Activation of Adenosine 2A receptor inhibits neutrophil apoptosis in an autophagy-dependent manner in mice with systemic inflammatory response syndrome. Sci Rep 2016, 6: 33614.

22. Crouch EE, Doetsch F. FACS isolation of endothelial cells and pericytes from mouse brain microregions. Nat Protoc 2018, 13: 738-751.

23. Rathmann D, Rijntjes E, Lietzow J, Köhrle J. Quantitative Analysis of Thyroid Hormone Metabolites in Cell Culture Samples Using LC-MS/MS. Eur Thyroid J 2015, 4: 51-58.

24. Wang Z, Liu F, Ye S, Jiang P, Yu X, Xu J, *et al*. Plasma proteome profiling of high-altitude polycythemia using TMT-based quantitative proteomics approach. J Proteomics 2019, 194: 60-69.

25. Devraj G, Guérit S, Seele J, Spitzer D, Macas J, Khel MI, *et al*. HIF-1α is involved in blood-brain barrier dysfunction and paracellular migration of bacteria in pneumococcal meningitis. Acta Neuropathol 2020, 140: 183-208.

26. Zhao L, Liu YW, Yang T, Gan L, Yang N, Dai SS, *et al*. The mutual regulation between miR-214 and A2AR signaling plays an important role in inflammatory response. Cell Signal 2015, 27: 2026-2034.

27. Liu YW, Zhao L, Zhou M, Wang H, Yang N, Dai SS. Transplantation with mGluR5 deficiency bone marrow displays antidepressant-like effect in C57BL/6J mice. Brain Behav Immun 2019, 79: 114-124.

28. Bajwa NM, Lee JB, Halavi S, Hartman RE, Obenaus A. Repeated isoflurane in adult male mice leads to acute and persistent motor decrements with long-term modifications in corpus callosum microstructural integrity. J Neurosci Res 2019, 97: 332-345.

29. Mao X, Qi S, Yu B, He J, Yu J, Chen D. Zn(2+) and L-isoleucine induce the expressions of porcine β-defensins in IPEC-J2 cells. Mol Biol Rep 2013, 40: 1547-1552.

30. Huang HC, Lin H, Huang MC. Lactoferrin promotes hair growth in mice and increases dermal papilla cell proliferation through Erk/Akt and Wnt signaling pathways. Arch Dermatol Res 2019, 311: 411-420.

31. Lai JJ, Cruz FM, Rock KL. Immune Sensing of Cell Death through Recognition of Histone Sequences by C-Type Lectin-Receptor-2d Causes Inflammation and Tissue Injury. Immunity 2020, 52: 123-135.

32. Drouin M, Saenz J, Chiffoleau E. C-Type Lectin-Like Receptors: Head or Tail in Cell Death Immunity. Front Immunol 2020, 11: 251.

33. Patin EC, Orr SJ, Schaible UE. Macrophage Inducible C-Type Lectin As a Multifunctional Player in Immunity. Front Immunol 2017, 8: 861.

34. Nikolakopoulou C, Willment JA, Brown GD. C-Type Lectin Receptors in Antifungal Immunity. Adv Exp Med Biol 2020, 1204: 1-30.

35. Ye XC, Hao Q, Ma WJ, Zhao QC, Wang WW, Yin HH, *et al*. Dectin-1/Syk signaling triggers neuroinflammation after ischemic stroke in mice. J Neuroinflammation 2020, 17: 17.

36. Fan Q, Tao R, Zhang H, Xie H, Lu L, Wang T, *et al*. Dectin-1 Contributes to Myocardial Ischemia/Reperfusion Injury by Regulating Macrophage Polarization and Neutrophil Infiltration. Circulation 2019, 139: 663-678.

37. Liu Q, Lin WJ, Tang Y. New Insights into the Dysfunctions of Pericytes and Neurovascular Units in Neurodegenerative Diseases. Neurosci Bull 2020, 36: 1570-1572.

38. Bhowmick S, D'Mello V, Caruso D, Wallerstein A, Abdul-Muneer PM. Impairment of pericyte-endothelium crosstalk leads to blood-brain barrier dysfunction following traumatic brain injury. Exp Neurol 2019, 317: 260-270.

39. Hesp ZC, Yoseph RY, Suzuki R, Jukkola P, Wilson C, Nishiyama A, *et al*. Proliferating NG2-Cell-Dependent Angiogenesis and Scar Formation Alter Axon Growth and Functional Recovery After Spinal Cord Injury in Mice. J Neurosci 2018, 38: 1366-1382.

40. Ojo J, Eisenbaum M, Shackleton B, Lynch C, Joshi U, Saltiel N, *et al*. Mural cell dysfunction leads to altered cerebrovascular tau uptake following repetitive head trauma. Neurobiol Dis 2021, 150: 105237.

41. Shah M, Yellon DM, Davidson SM. The Role of Extracellular DNA and Histones in Ischaemia-Reperfusion Injury of the Myocardium. Cardiovasc Drugs Ther 2020, 34: 123-131.

42. Szatmary P, Huang W, Criddle D, Tepikin A, Sutton R. Biology, role and therapeutic potential of circulating histones in acute inflammatory disorders. J Cell Mol Med 2018, 22: 4617-4629.

43. Rada B. Neutrophil Extracellular Traps. Methods Mol Biol 2019, 1982: 517-528.

44. Yousefi S, Stojkov D, Germic N, Simon D, Wang X, Benarafa C, *et al*. Untangling "NETosis" from NETs. Eur J Immunol 2019, 49: 221-227.

45. Fu X, Zeng H, Zhao J, Zhou G, Zhou H, Zhuang J, *et al*. Inhibition of Dectin-1 Ameliorates Neuroinflammation by Regulating Microglia/Macrophage Phenotype After Intracerebral Hemorrhage in Mice. Transl Stroke Res 2021, 12: 1018-1034.

46. Li X, Utomo A, Cullere X, Choi MM, Milner DJ, Venkatesh D, *et al*. The β-glucan receptor Dectin-1 activates the integrin Mac-1 in neutrophils via Vav protein signaling to promote Candida albicans clearance. Cell Host Microbe 2011, 10: 603-615.

Figures

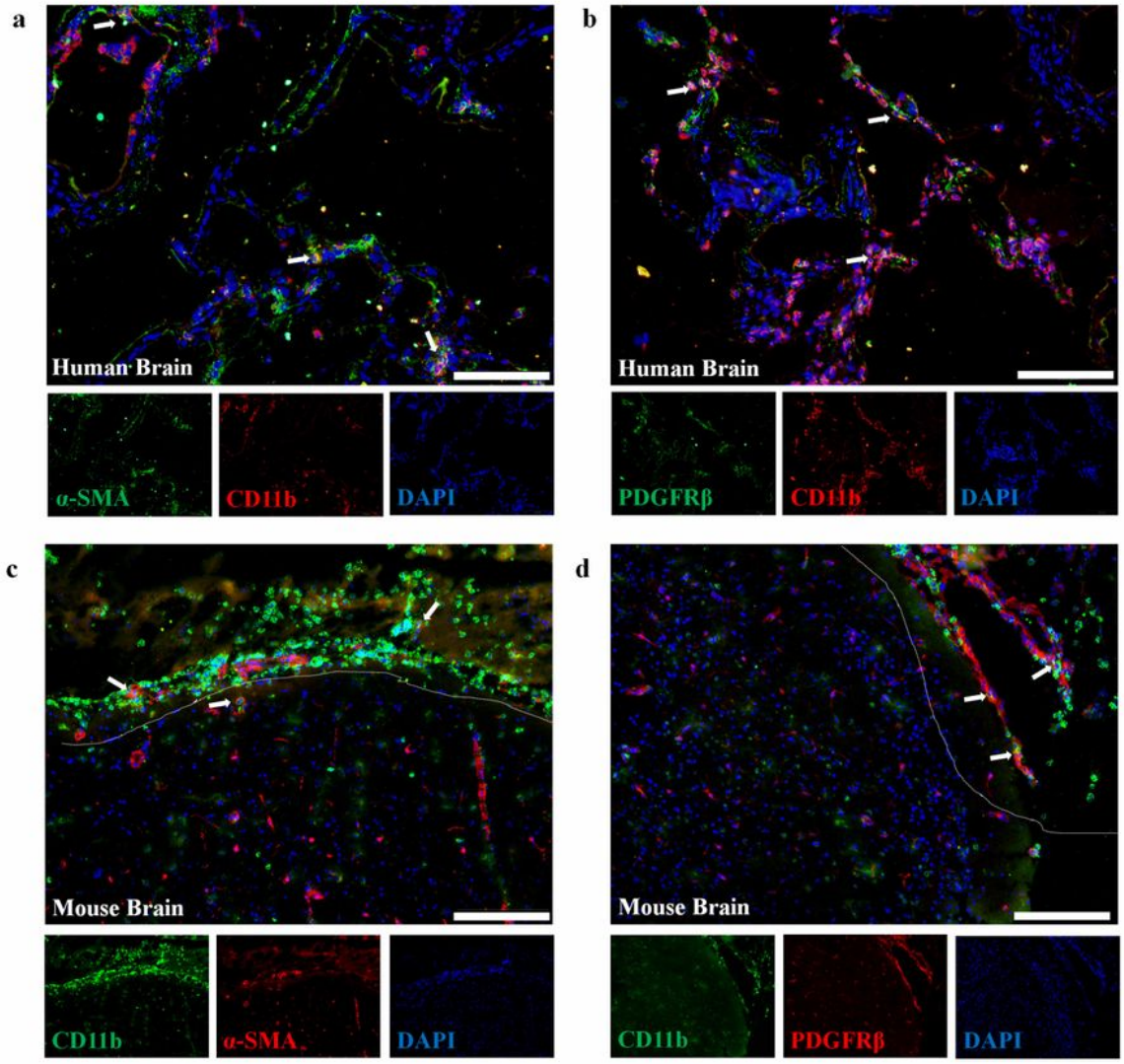

Figure 1

Immunofluorescence of PDGFRβ and CD11b in damaged brain tissue. **a&b** Immunostaining of pericyte marker (PDGFRβ/α-SMA, green) and CD11b (red) in brain tissues from TBI patient. **c&d** Immunostaining of pericyte marker (PDGFRβ/α-SMA, red) and CD11b (green) in brain tissues from TBI mouse. Damaged tissues were marked with dotted lines. Human and mouse brain tissues were collected within 24-48 hours after TBI. White scale bar represents for 100μm. Cell nucleus were stained with DAPI (blue).

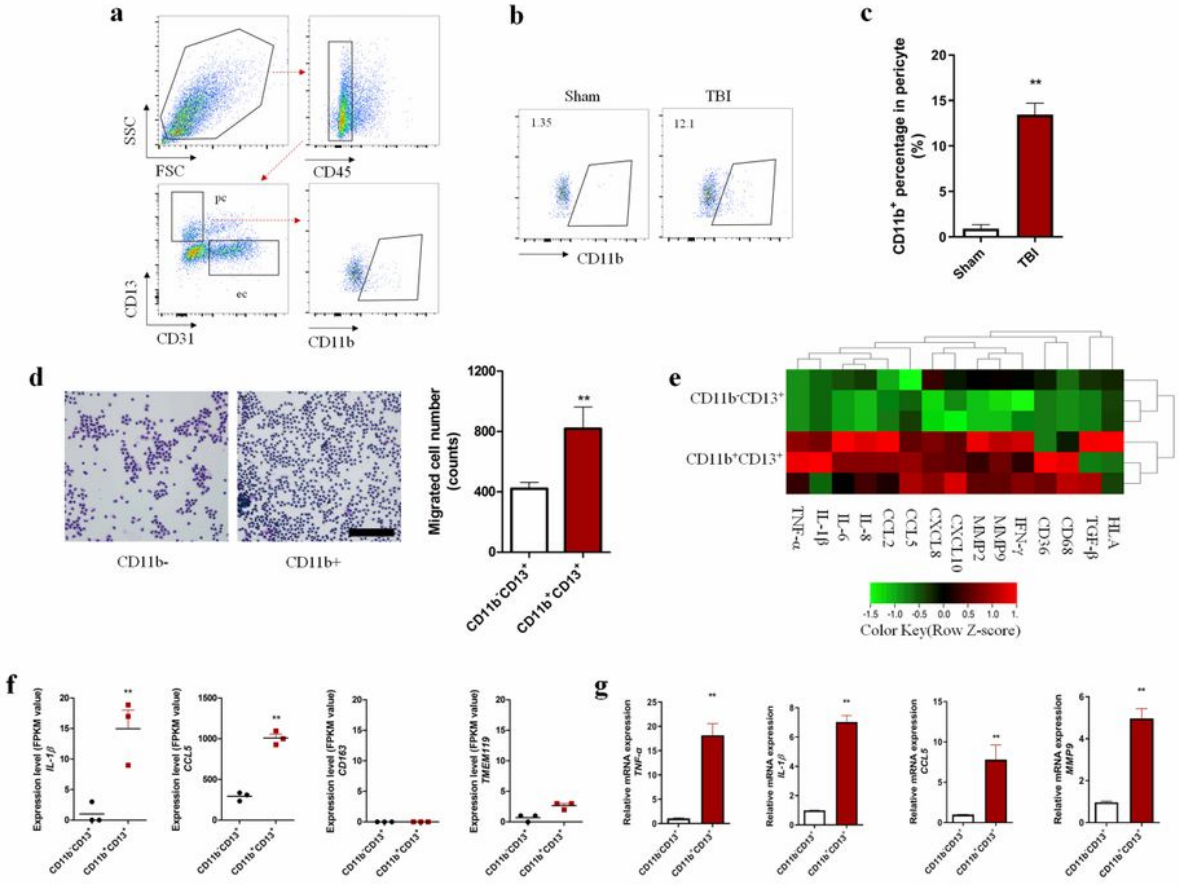

Figure 2

Functional and molecular features of CD11b positive pericyte. **a** Flow cytometric diagram of $CD11b^+$ pericytes in brain tissues. **b** Plots of $CD11b^+$ pericytes from Sham and TBI mice. **c** Quantification of $CD11b^+$ pericytes in brain tissues from Sham and TBI mice. (n=5 for each group). **d** Neutrophil migration experiment mediated by $CD11b^+$ and $CD11b^-$ pericytes. Black bar represents 100μm. **e** RNA-

sequencing data of sorted cells ($CD11b^+CD13^+$ and $CD11b^-CD13^+$) from damaged brain tissues. Red represents for high-expression, green represents for low-expression, black stands for even expression between these two subsets. **f** Expression levels (FPKM value) of cytokine(*IL-1β*), chemokine(*CCL5*), macrophage marker(*CD163*), and microglia marker (*TMEM119*) in sorted cells. **g** Relative mRNA levels of target genes in $CD11b^+$ population compared to $CD11b^-$ pericytes. Data were shown as mean±SEM, presented for 3-5 individual experiments and analyzed by two-tailed unpaired Student's *t* test. $^{**}p<0.01$.

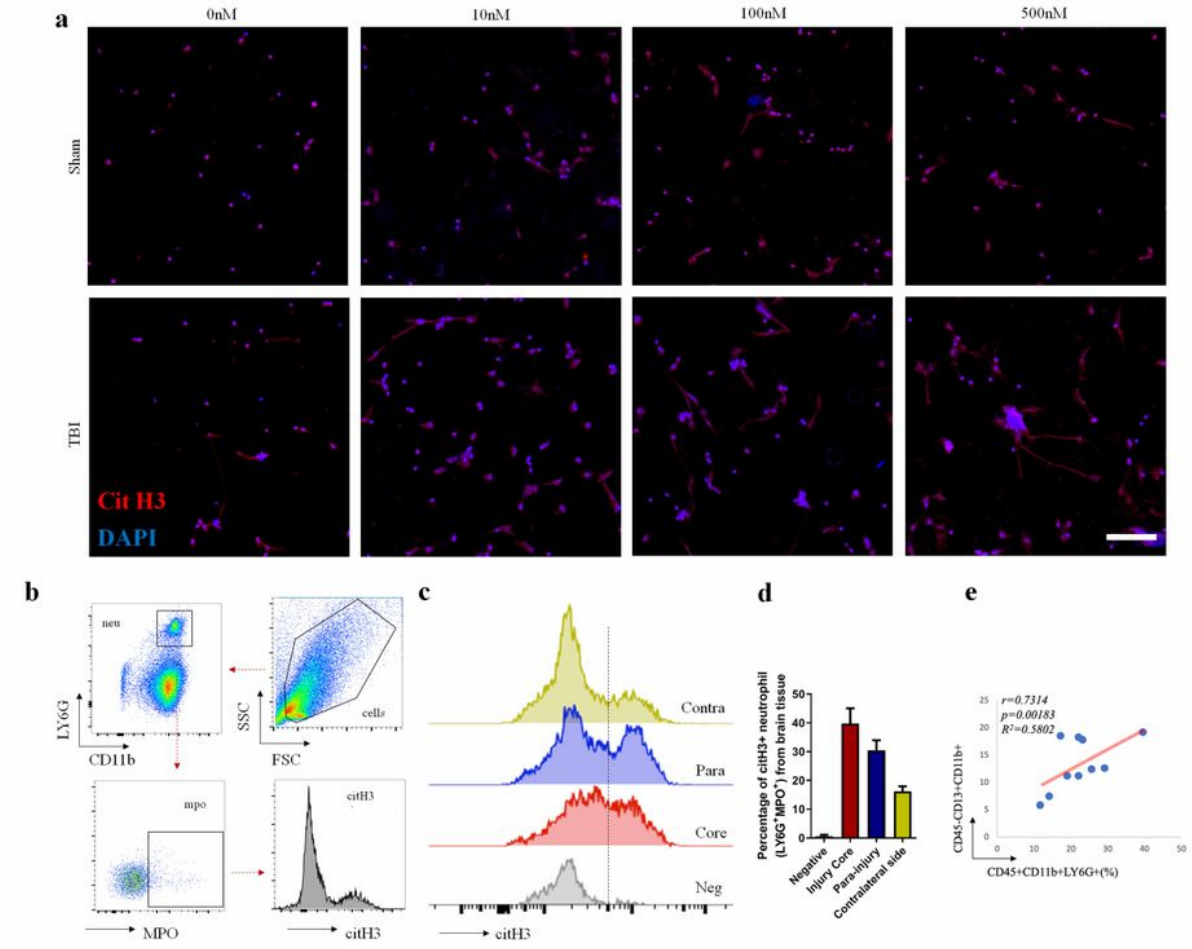

Figure 3

NETs formation after TBI. **a** Immunofluorescence of NETs formation from peripheral blood. The neutrophils were isolated from peripheral blood of Sham and TBI mice at 24 hours post injury. Then the neutrophils were treated with gradient concentrations of PMA (10 ng/ml, 100 ng/ml, 500 ng/ml) for 6 hours and stained with Cit H3(red) and DAPI(blue). White scale bar represents for 100μm. **b** Flow cytometric diagram of NETs formation ($CitH3^+LY6G^+MPO^+$) in brain tissues. **c** Cit H3 levels in MPO^+ neutrophils from different brain tissues post TBI. Negative for $LY6G^+MPO^+$neutrophils stained without Cit H3 antibody. Brain tissues were collected from injury core, para-injury side and injury contralateral side of TBI mice. **d** Quantification of Cit H3 positive neutrophils in (c). Each bar represents 3 individual experiments. Data were shown as mean±SEM. **e** Correlation analysis between neutrophil percentage and CD11b+ pericyte frequency in damaged brain, n=10.

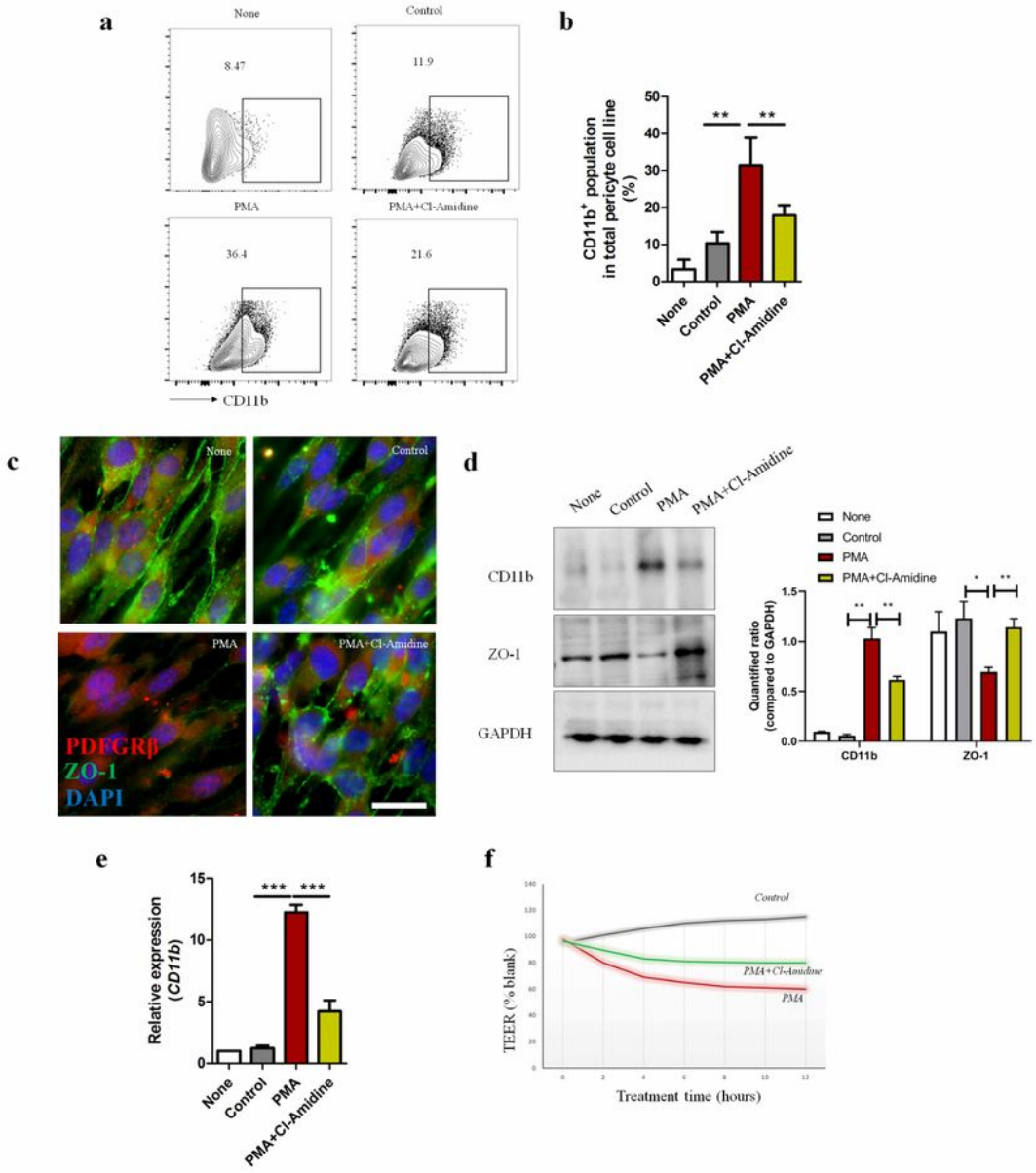

Figure 4

Effects of NETs-formed medium on pericyte. Murine brain pericyte cell line MBVP was incubated with specific mediums for 48 hours. None means normal medium, control means medium from non-stimulated neutrophils, PMA means NETs-formed medium stimulated by PMA (100ng/ml), PMA+Cl-Amidine means medium from PMA stimulation (100ng/ml) combined with NETs inhibitor Cl-Amidine (10μM). Supernatant was collected by centrifugation for removing neutrophils. **a** Cytometric analysis of

$CD11b^+$ MBVP after different treatments. **b** Quantification of $CD11b^+$ MBVP percentage in (a), n=3. **c** Immunostaining of tight junction protein (ZO-1, green) and pericyte marker (PDGFRβ, red) on MBVP. White scale bar represents for 20μm. **d** WB of CD11b and ZO-1 expression in MBVP after different treatments. Protein levels were quantified by comparing to loading control GAPDH. **e** Realtime-PCR analysis of CD11b relative mRNA levels in different treatment groups compared to none group. Each group contains 5 individual experiments. **f**Representative graph of continuous TEER values of MBVP incubated with intended culture medium. TEER values of each group were compared to blank (MBVP under normal culture medium). Data were shown as mean±SEM and analyzed by ANOVA. *p<0.05, **p<0.01, ***p<0.001.

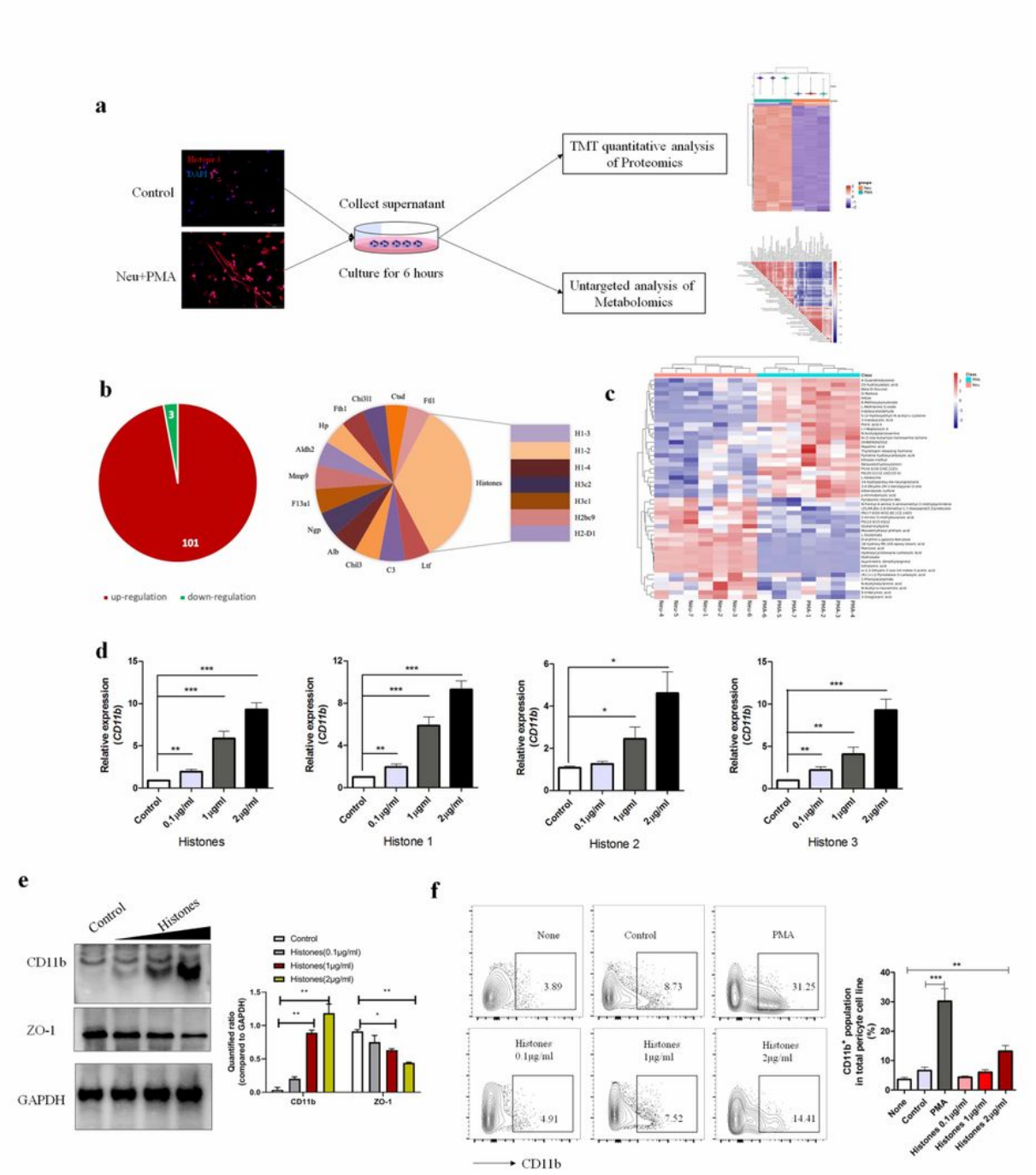

Figure 5

Analysis of functional components from NETs-formed medium affecting pericyte phenotype. **a** Workflow for proteomics and metabolomics comparisons between NETs-formed medium (PMA) and control medium (neutrophils without PMA stimulation). Proteomics n=3 for each group. Metabolomics n=7 for each group. **b** Pie chart of differential proteins and top 20 up-regulated proteins in NETs-formed medium. Changes greater than 1.5-fold and $p < 0.05$ were considered significantly differential. **c** Hierarchical

clustering of differential metabolites in NETs-formed medium. Differential molecules repeatedly consistent in the same group with p value<0.05 were screened out and highlighted in red (up-regulated) and blue (down-regulated). **d** Realtime-PCR analysis of CD11b relative mRNA expression in histone-treated MBVP compared to control MBVP. Recombinant histone peptides were treated with cells for 24 hours. Histones represent mixture of histone 1, histone 2 and histone 3 at the ratio of 1:1:1. **e** WB analysis of CD11b and ZO-1 in MBVP incubated with histones for 48 hours. Protein levels were quantified by comparing to GAPDH. **f** FACS analysis of $CD11b^{+}$ percentage of MBVP incubated with specific conditions for 48 hours. Data were shown as mean±SEM, presented for 3 individual experiments and analyzed by ANOVA. *p<0.05, **p<0.01, ***p<0.001.

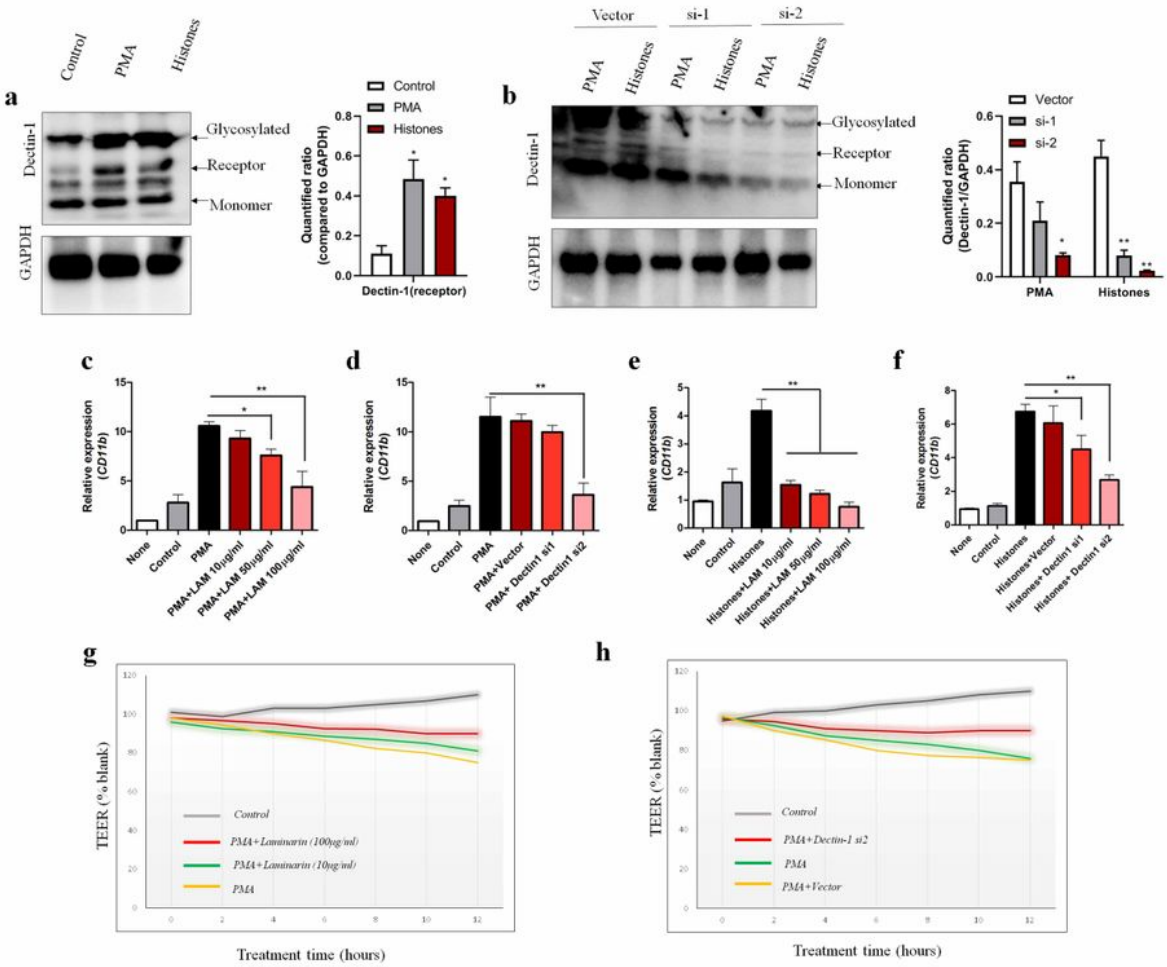

Figure 6

Expression and function of Dectin-1 on brain pericyte. Specific medium: Control means medium from non-stimulated neutrophils, PMA means NETs formation medium from neutrophils stimulated by PMA (100ng/ml), Histones means mixed purified histone peptides (H1: H2:H3=1:1:1) were dissolved at 2μg/ml. **a** WB analysis of Dectin-1expression on pericyte cell line MBVP incubated with specific medium for 48 hours. The specific medium was mixed with normal culture medium at the ratio of 1:3 as described

above. **b** WB analysis of Detin-1 expression on MBVP stimulated with specific medium after transfecting blank vector or Dectin-1 siRNAs (si-1, si-2). Dectin-1 protein levels were quantified by comparing to GAPDH. **c** Relative CD11b mRNA expression on MBVP (compared to none group) after NETs-formed medium treatment combined with indicated concentration of Dectin-1 antagonist LAM for 24 hours. **d**Relative CD11b mRNA expression on MBVP after NETs-formed medium treatment combined with Dectin-1 siRNAs transfection for 24 hours. Vector means adding transfection solution without siRNAs. **e** Relative CD11b mRNA expression on MBVP (compared to none group) after Histones (2μg/ml) treatment combined with indicated concentration of Dectin-1 for 24 hours. **f** Relative CD11b mRNA expression on MBVP after Histones (2μg/ml) treatment combined with Dectin-1 siRNAs transfection for 24 hours. Vector means adding transfection solution without siRNAs. **g**Representative graph of continuous TEER values on MBVP treated by NETs-formed medium combined with/without Dectin-1 antagonist Laminarin. **h** Representative graph of continuous TEER values on MBVP treated by NETs-formed medium combined with/without Dectin-1 siRNA transfection. TEER values of each group were compared to blank (MBVP under normal culture medium). Data were shown as mean±SEM, presented for 5 individual experiments and analyzed by One-way ANOVA. *p<0.05, **p<0.01.

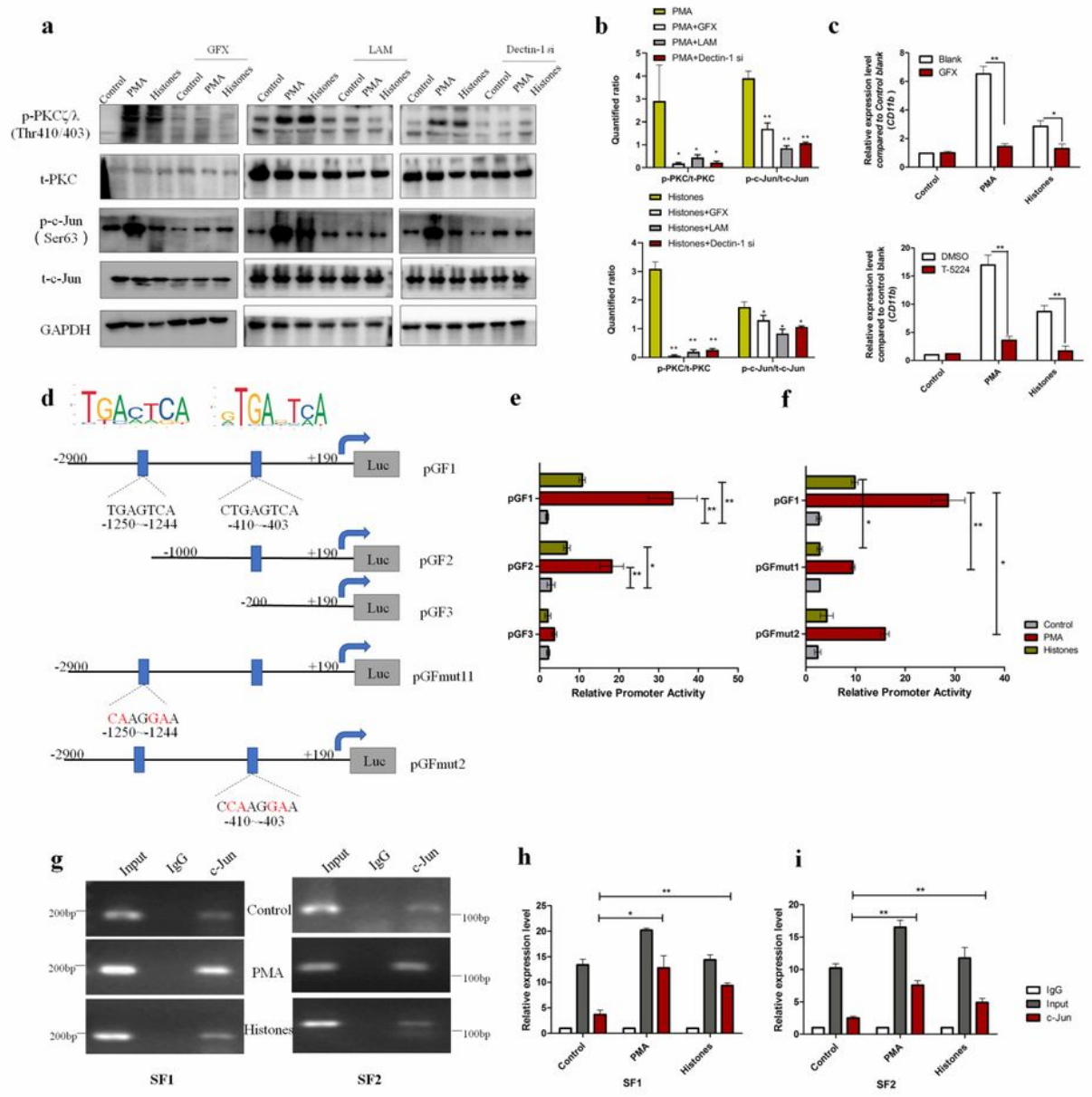

Figure 7

PKC/c-Jun/CD11b pathways in histones/Dectin-1 recognition. **a** WB analysis of total PKC (t-PKC), phosphorylated-PKCζ/λ (p- PKCζ/λ), total c-Jun (t-c-Jun) and phosphorylated-c-Jun in MBVP treated with NETs-formed medium (PMA) or Histones (2μg/ml) combined with or without PKC inhibitor GFX (5μM), Dectin-1 antagonist LAM (100μg/ml) and siRNAs for 24 hours. **b** Quantified ratios of p-PKC/t-PKC and p-c-Jun/t-c-Jun in specific groups. Comparisons were made between PMA/Histones and combined

treatment groups. **c** Relative expression of CD11b mRNA (compared to control blank group) on MBVP treated with NETs-formed medium (PMA) and Histones (2μg/ml) for 24 hours in the presence of GFX (PKC inhibitor, 5μM) or T-5224 (c-Jun inhibitor, 10μM). **d** Putative c-Jun binding sequence of mouse CD11b promoter gene. **e** Luciferace activity of MBVP co-transfected with indicated reporters under specific conditions. **f** Luciferace activity of MBVP co-transfected with mutated reporters under specific conditions. All transfected cells were treated under indicated conditions for 24 hours and lysed for dural-luciferace measurement. **g** CHIP assays of c-Jun binding sequence from murine *CD11b* promoter gene. After treating MBVP with indicated conditions for 24 hours, the total chromatin was collected and amplified as input (positive control). Antibody against c-Jun was used for pulling down the biding segments, of which IgG was introduced as negative control. Two pairs of specific primers that covered each binding site were used to amplify SF1 contained segment (-1250~-1244) and SF2 contained segment (-410~-403) respectively within 30 cycles. **h&i** Realtime-PCR of CHIP products. The quantitative Realtime-PCR was performed with GAPDH as internal reference gene and regarded IgG in each group as control. Data were shown as mean±SEM, presented for 3 individual experiments and analyzed by two-tailed unpaired Student's *t* test or ANOVA. $^{**}p<0.01$, $^{*}p<0.05$.

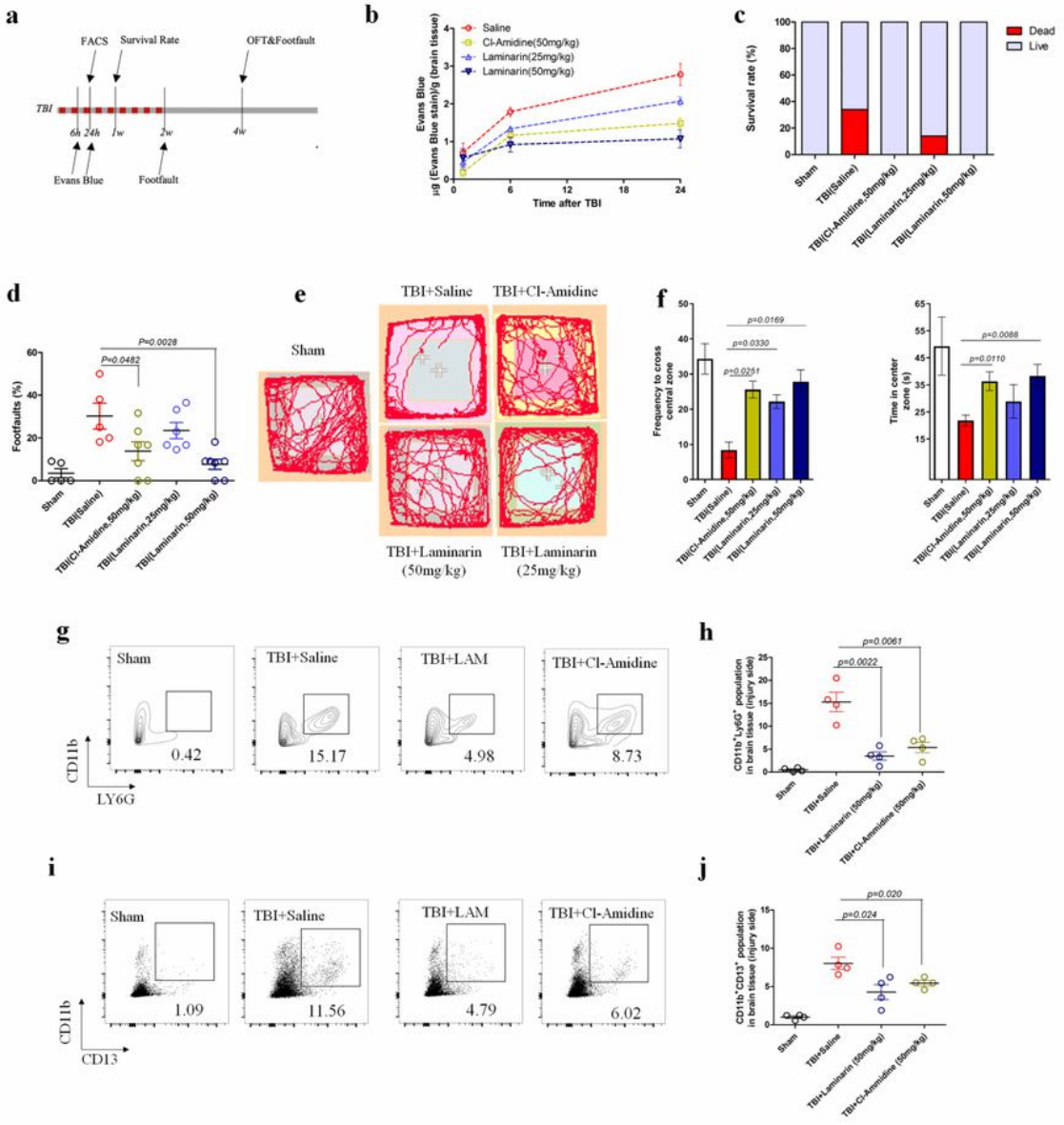

Figure 8

Evaluations of BBB integrity, pericyte activation, neutrophil infiltration and neurological recovery by targeting at NETs-Dectin-1 axis post TBI. **a** Schematic workflow of animal experiments. After constructing moderate brain impact model, mice were immediately treated with NETs inhibitor Cl-Amidine (50mg/kg) and Dectin-1 antagonist Laminarin (25mg/kg and 50mg/kg) by intraperitoneal injection every three days (5 injections). Two weeks later (red points marked), the treatments were terminated and mice were fed

without any interferences. **b** Quantification of Evan Blue in left brain hemisphere. Each group contains 4 mice for each group at intended time point. **c** Survival rate of each group at the first week after TBI impact in the presence of different treatments. n=6 for Sham, n=10 for TBI. **d** Footfault evaluation of TBI mice with administration of indicated drugs at 2 weeks post injury. n≥5 for each group. **e** Tracing records of mice movement in OFT assessment at 4 weeks after moderate TBI impact in the presence of different treatments. **f**Quantification of OFT assessment (e) in the aspects of frequency to cross central zone and time that mice spent in center zone. n≥5 for each group. **g** FACS analysis of infiltrated neutrophils ($CD45^+CD11b^+LY6G^+$) from injured brain tissue at 24 hours in TBI mice treated with indicated drugs. n=4 for each group. **h** Quantification of neutrophils in brain tissues from each group, n=4. **i** FACS analysis of $CD11b^+$ brain pericyte ($CD45^-CD11b^+CD13^+$) from brain tissue of TBI mice treated with indicated drugs. n=4 for each group. **j** Quantification of $CD11b^+$ brain pericyte in brain tissues from each group, n=4. Data are presented as mean±SEM, and analyzed by ANOVA. The animal numbers and *p* values of each group are shown in figures and intended legends.

Supplementary Files

This is a list of supplementary files associated with this preprint. Click to download.

- FigureS1.jpg
- FigureS2.jpg
- FigureS3.jpg
- FigureS4.jpg
- FigureS5.jpg
- FigureS6.jpg
- supplementaryinformationlegends.docx
- Supplementarytables1.docx